

Cell Line Classification Using Electric Cell-substrate Impedance Sensing (ECIS)

Megan L. Gelsinger¹, Laura L. Tupper², and David S. Matteson³

¹Department of Statistical Science, Cornell University, Ithaca, NY 14853 (email: m1g276@cornell.edu)

²Department of Mathematics and Statistics, Williams College, 33 Stetson Court, Williamstown, MA 01267
(email: 11t1@williams.edu)

³Departments of Statistical Science and Social Statistics, Cornell University, Ithaca, NY 14853 (email:
matteson@cornell.edu)

February 12, 2023

Abstract

We consider cell line classification using multivariate time series data obtained from electric cell-substrate impedance sensing (ECIS) technology. The ECIS device, which monitors the attachment and spreading of mammalian cells in real time through the collection of electrical impedance data, has historically been used to study one cell line at a time. However, we show that if applied to data from multiple cell lines, ECIS can be used to classify unknown or potentially mislabeled cells, which may help to mitigate the current crisis of reproducibility in the biological literature. We assess a range of approaches to this new problem, testing different classification methods and deriving a dictionary of 29 features to characterize ECIS data. Our analysis also makes use of simultaneous multi-frequency ECIS data, where previous studies have focused on only one frequency. In classification tests on fifteen mammalian cell lines, we obtain very high out-of-sample accuracy. These preliminary findings provide a baseline for future large-scale studies in this field.

Keywords: biophysics, classification analysis, multivariate time series, supervised learning

1 Introduction

In the 1990's, Giaever and Keese introduced ECIS as a label-free, real-time, electrical impedance-based method for studying cell behavior in tissue culture [1]. In this work, the group provided both the models and a basic blueprint for the device needed to implement ECIS. The device they proposed consisted of a typical cell culture plate, in which each well was fitted with a gold electrode, allowing for the passage of electrical currents at various AC frequencies. After application of such currents, the device could then measure the electrical impedance associated with each current as a function of time and divide it into its components resistance and capacitance, allowing for live monitoring of mammalian cell activity.

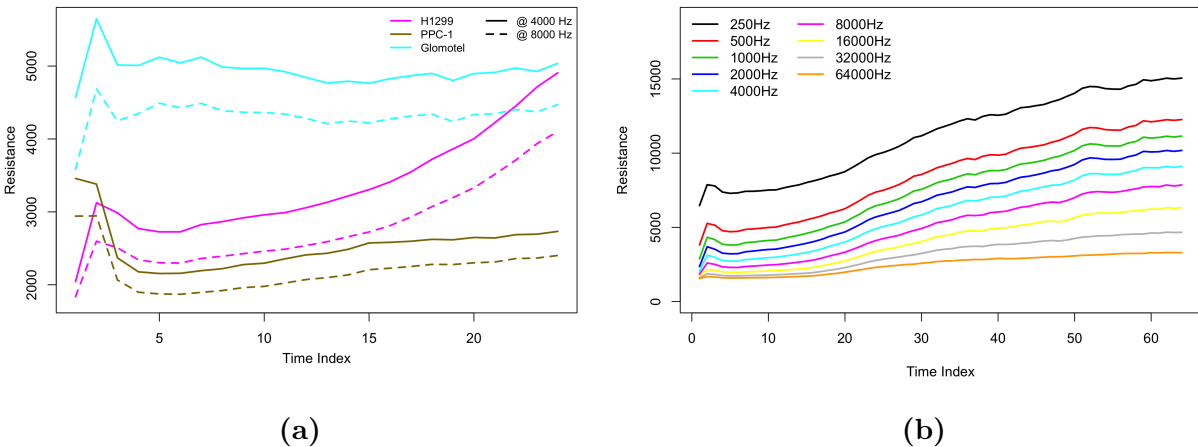


Figure 1. Visualizing ECIS Data: Resistance measurements as recorded by an ECIS[®] device. (a) A single response for each of three different cell lines, each exposed to two different AC frequencies. (b) Response of H1299 cell line to all nine AC frequencies.

In seeking to expand the scope of ECIS technology to include cell identification and classification, we continue a long history of finding innovative ways to use the original design proposed by Giaever and Keese. Since its introduction, researchers in biotechnology have studied ways of improving the overall efficiency and effectiveness of ECIS devices through experimenting with the design scheme [2]. Others in the field have constructed specially tuned versions of an ECIS device for specific applications in cancer cell and clinical diag-

nostic research [3, 4]. Giaever and Keese even went on to manufacture their own series of ECIS[®] devices.

Other studies have used the technology to monitor the activity of cells grown in tissue culture. Early research focused on showing that ECIS measurements could be associated with known biological characteristics of a particular cell line from the attachment and spreading phases of growth [5, 6]. More recently, others have used ECIS to study a cell line before and after an event, such as exposure to cytotoxins, and evaluate induced differences [7, 8]. For a more complete overview of the use of ECIS in the biological literature see [9].

Generally, previous studies have focused on only one cell line at a time, and have neglected the full potential of multiple frequency measurements available through a standard ECIS[®] device when trying to characterize the cell line. Lo et al. (2007) consider two different cell lines, one cancerous and one healthy, but their analysis relied on only one frequency of data and did not extend to additional cell types [10]. Huang et al. (2009) consider multiple frequencies in their analysis of cytotoxic effects on cell morphology, but they limit their use of the multivariate data to a single time index and only one cell line [7]. While these approaches have been sufficient for the scope of studies to date, a broader consideration of ECIS data may open greater opportunities, including new approaches for ECIS-based cell line identification.

The main application of ECIS data we consider is cell line classification. Biological studies often rely upon cultured mammalian cells, which are known to mutate or become misclassified during the life of an experiment. When such anomalies go unnoticed, erroneous results are reported, contributing to the multi-billion dollar irreproducibility problem [11]. While previous studies, such as those above, have suggested specific features to help characterize single cell lines, none have employed statistical techniques to quantify the ability of potential characteristic features to simultaneously classify multiple cell lines; the typical statistical analysis in these studies only considered t -tests and F -tests to measure differences in the mean value of a specific feature across populations. This is fundamentally different than

performing classification based on a feature, as the latter technique simultaneously measures the characteristic across all populations, and quantifies how well it separates and identifies the groups. While we ultimately aim to develop an integrated system to perform cell line classification, that will require much more data collection, and we limit the scope of this manuscript to a preliminary analysis. We extract many previously considered cell-specific ECIS characteristics from a standard ECIS[®] device, measure them across both time and AC frequency, and quantify their classification performance through established statistical techniques including classification trees, regularized discriminant analysis (RDA), and two special cases of RDA, linear discriminant analysis (LDA), and quadratic discriminant analysis (QDA).

The remainder of this paper provides the details of our study. In sections 2 and 3, we describe our dataset, and feature specification, respectively. In section 4, we discuss the classification analysis results, and in section 5 we offer conclusions, and discuss avenues for future work.

2 ECIS Data and Experimental Design

The dataset considered throughout this paper was provided by Applied BioPhysics, the proprietor of ECIS[®], as recorded by one of their 96-well ECIS[®]Z θ devices. It consists of fourteen replicates of fifteen different mammalian cell lines grown on two different serums (gel and bovine serum albumin (BSA)). The data will be grouped (and compared) by serum type in our forthcoming analysis. Each observation was exposed to nine different electrical current frequencies over the course of 20 hours, resulting in 64 approximately evenly spaced measurement times. The fifteen different cell lines are: HUTU80, CHOK1, MDCKII, LCELL, WI-38, VA-13, NRK, PPC-1, DuPro, Glomotel, BSC1, DU145, H1299, NIH3T3, and PC-3. The nine AC frequencies measured are: 250, 500, 1000, 2000, 4000, 8000, 16000, 32000, and 64000 Hz. Each 96-well plate held three different cell lines; for each line, we considered data

from one plate. Impedance measurements were recorded approximately once every 20 minutes across all nine AC frequencies (see Figure 1 (b)). The impedance measurements were decomposed into resistance and capacitance according to the model described in Giaever and Keese [1].

3 Feature Specification

3.1 Technical Review

Many of the characteristics identified in the literature as varying by cell line or cell condition were extracted from data obtained during confluence, or the steady-state portion of growth following the initial growth and spreading stages. During this phase, the well is completely covered with cells, allowing for only minute movements. Data collection commonly began after 20-24 hours, once cells had reached confluence, and continued for about 20 hours at a fine sampling frequency, ranging from every two minutes to every second depending on the study. With this resolution of data, researchers were able to extract features such as:

- the slope parameter β characterizing a least-squares straight-line fit to a log-log plot of power spectrum versus frequency ν [6, 7, 8, 10, 12]; e.g., Brownian noise displays an ν^{-2} power law, with $\beta = 2$;
- the sample kurtosis, a measure of distributional shape [10];
- the first e^{-1} crossing of the autocorrelation function of the noise time series from confluence onward (extracted from resistance time series over same time period), to estimate the exponential decay time [8, 10].

Two other post-confluence features suggested in previous works were R_b and α . R_b reflects the barrier resistance between cells, whereas α reflects the constraint on current flow beneath

the cells (see Figure 2 for visualization). R_b and α are defined by the following relationships:

$$\frac{1}{Z_c(\nu)} = \frac{1}{Z_n(\nu)} \left(\frac{Z_n(\nu)}{Z_n(\nu) + Z_m(\nu)} + \frac{\frac{Z_n(\nu)}{Z_n(\nu) + Z_m(\nu)}}{\frac{\gamma r_c}{2} \frac{I_0(\gamma r_c)}{I_1(\gamma r_c)} + R_b \left(\frac{1}{Z_n(\nu)} + \frac{1}{Z_m(\nu)} \right)} \right); \quad (1)$$

$$\gamma r_c = r_c \sqrt{\frac{\rho}{h} \left(\frac{1}{Z_n(\nu)} + \frac{1}{Z_m(\nu)} \right)} = \alpha \sqrt{\frac{1}{Z_n(\nu)} + \frac{1}{Z_m(\nu)}}. \quad (2)$$

For frequency ν , $Z_c(\nu) > 0$ is the impedance (per unit area) of the cell-covered electrode, $Z_n(\nu)$ is the impedance of the cell-free (empty, reference) electrode, $Z_m(\nu)$ is the membrane impedance of the cells, r_c is the radius of the cell, ρ is the resistivity of the solution, h is the height of the space between the ventral surface of the cell and the substrate, and I_0 and I_1 are the modified Bessel functions of the first kind in order 0 and 1 [1].

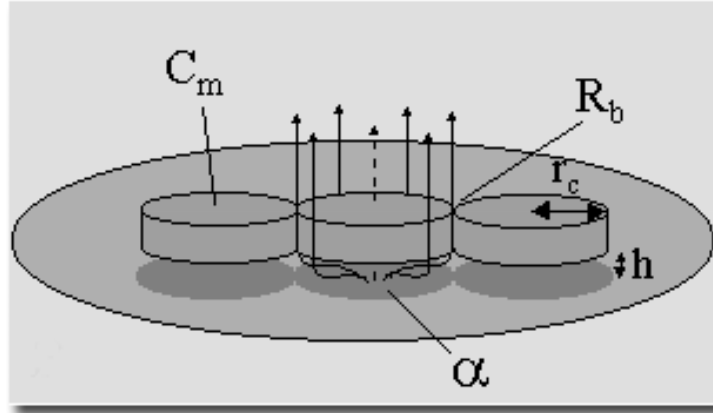


Figure 2. Visualizing the ECIS Model: Image obtained from Applied BioPhysics' website (biophysics.com). In the ECIS model, cells are viewed as disks, characterized by parameters R_b , α , r_c , C_m , and h .

An ECIS[®] device is incapable of recording all of the parameters in equations (1) - (2). Instead, it records only $Z_c(\nu)$ and $Z_n(\nu)$ over a set of frequencies $\{\nu_1, \dots, \nu_k\}$, with $k \geq 3$, and estimates the values of $Z_m(\nu)$, R_b and α which fit the data best. Since these optimal values cannot be computed analytically, the ECIS[®] software uses the Nelder-Mead downhill simplex method to select a series of parameter values. From there, the program calculates the mean square error between the measured and modeled frequency scan values, and returns

the set of parameter values which minimize this error. The absolute error is normalized to the cell-free reference, so the frequencies are appropriately weighted. It is important to note that influencing these equations and calculations are the assumptions that the ECIS model can be understood as a series RC circuit, with cells represented by circular discs hovering above (not directly touching) a gold electrode. We consider R_b and α as characteristics which may differentiate cell lines, as they were considered by both [1] and [7] in their analyses.

Several previous studies also evaluated features that were specific to the attachment and spreading phases of growth. In particular, some researchers found that certain cell lines “peaked higher” and “increased more rapidly” during these initial stages of growth [13, 14]. Additional remarks are very limited as the majority of prior studies concentrated less on attachment and spreading and more on confluence behavior.

The statistical analysis involved in these studies focused on t -tests and F -tests to look for significant differences in a feature’s mean value across populations of interest. For example, when Opp et al. (2009) considered whether a particular cell population inoculated with varying degrees of a cytotoxin had differing mean R_b values for each dosage level, the authors performed Student’s t -test for two samples with unequal variance, for pairs of dosages, such as 5 μ M versus 10 μ M of cytotoxin [7]. Another example came from the comparison of cancerous and noncancerous cells, in which an F -test was conducted to assess the probability of the two cell lines coming from the same distribution, given the means and variances of their power slopes β [10].

3.2 Feature Space Specification

The design for our study did not emphasize the confluence stage of growth; only twelve observations per frequency were recorded during this stage, by sampling wells once every 20 minutes over four hours in the confluence phase. This compares to the thousands of observations available for a single frequency in previous confluence phase studies. Given the lack of data available during this final steady-state stage, we did not extract many of the

confluence region features mentioned in Section 3.1. The only exceptions were R_b and α . Computationally only one time index worth of data during the confluence region is needed to approximate these values; at this single time index, the data from all measured frequencies are combined to estimate R_b and α . Since we had twelve time indices worth of data, though, we averaged the R_b and α at each of these twelve points to get more accurate estimates of the overall R_b and α .

To extend our feature space, we also included proxies for those features from the attachment and spreading portions of cell growth mentioned in Section 3.1. These included:

- i. End of run resistance value (EOR);
- ii. Maximum resistance value (MR);
- iii. Resistance at two hours (R2h).

Beyond the features described above, we extended our feature space in a novel way. Previous studies involving these features evaluated them at only one frequency, typically 4000 Hz. One of the main advantages of ECIS[®]Z θ , though, is its ability to record multi-frequency data. Therefore, we include relevant features (EOR, MR, R2h) at all nine measurement frequencies given in Section 2. This gives us a total of $(3 \times 9) + 2 = 29$ characteristics in our feature space which we utilize in our classification analysis below.

4 ECIS-based Cell Line Classification Analysis

Classification algorithms provide predictive accuracy rates which reflect quantitatively how well certain characteristics differentiate the data. In previous ECIS related works, none of these algorithms were used to assess features for general cell line classification; instead, F -tests and t -tests were relied upon to determine whether the mean value of the feature in question differed by group. We consider a series of classifiers in our study to provide this missing quantitative evaluation of potential features for cell line classification.

Classification analysis was performed using several different supervised learning methods on several different combinations of features. The first “grouping” of features considered was similar to that of previous works, where each feature was analyzed on an individual basis as a tool for cell line differentiation. We also considered all pairs and trios of our 29 features to determine if any provided better separation of the data, and if so, by how much. All combinations of features were evaluated using both classification trees and RDA (with LDA and QDA as special cases).

As mentioned in Section 2, we treated those cells inoculated in gel and BSA serums differently, looking to gain insight on the conditions which promote optimal cell line classification. The analysis that follows provides an in-depth description and visualization of the classification procedures performed on the gel-based cells. The same procedures were performed on BSA-based cells; we provide a highlighted summary of these results and comparison to the gel-based cell results at the conclusion of this section.

4.1 Classification Trees

We began our analysis of the gel-based cells with classification trees, as they use the most elementary division of the feature space to classify observations into groups. Classification trees perform an iterated series of binary splits on the data space to assign each observation in a given region to the most commonly occurring class of training observations in that region. To create these splits, we select the predictor, or feature, X_j with cutpoint s such that splitting the feature space into regions $\{X|X_j < s\}$ and $\{X|X_j \geq s\}$ leads to the greatest possible reduction in a particular metric. Several different metrics exist for assessing the quality of a particular split, arguably the most common of which is the Gini index, defined by

$$G = \sum_{k=1}^K \hat{p}_{mk}(1 - \hat{p}_{mk}).$$

Here we assume the data can be divided into K classes, with \hat{p}_{mk} representing the portion of training observations in the m th region that are from the k th class. The Gini index, therefore, represents a measure of the total variance across the K classes, which is often referred to as node purity; G assumes small values, or is “pure,” when \hat{p}_{mk} is near zero or one, meaning nearly none or nearly all of the training observations in the m th region are from the k th class, respectively. So, to construct a binary split, we consider all predictors X_1, \dots, X_p at all possible values s , and select the feature and cutpoint such that G is minimized. A classification tree is built by iteratively performing these splits on training data until reaching a specified node purity threshold. A test set can then be read into the tree, and a predictive accuracy rate computed [15]. We note that based on their definition, the splits in classification trees divide the feature space into a series of half-planes, or rectangles in 2D.

We constructed classification trees on the data, using each single, pair, and trio of features as predictors in separate models. We randomly split the entire dataset for each cell line in half, using seven of the fourteen available observations in the training set and the remaining seven in the test set. For each individual feature we then constructed classification trees using the `tree()` function in R on the training set and assessed the out-of-sample classification predictive accuracy rate using `predict.tree()` on the test set. We repeated this analysis on twenty different random splits of the data into training and testing sets. Reported accuracy rates for each feature are the average over all twenty of these trials. This procedure was continued with all distinct pairs and trios of features.

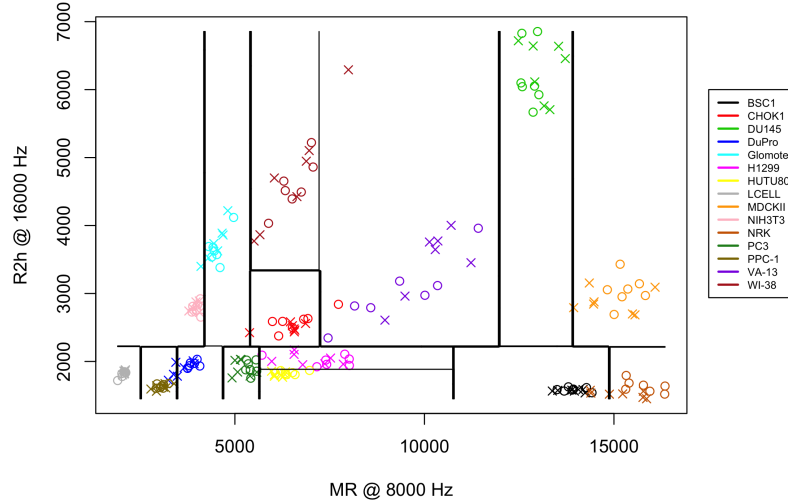
Table 1 reflects the best feature(s) for classification based on the average accuracy rate. While the features highlighted in Table 1 may not be the overall best, since, again, their associated classification accuracies are just estimates, EOR, MR, and R2h repeatedly appeared at similar mid- to high-range frequencies when replicating our procedure. We also note that the features highlighted in Table 1 are the best by a small margin; at least 10% of all the single, pairs and trios of features were within 5% of the best respective classification rate.

Feature Space Dimension	Selected Classification Feature(s)	Out-of-Sample Classification Rate	Approximate Standard Error
1	EOR @ 2000 Hz	0.714	0.009
2	R2h @ 32000 Hz ; MR @ 8000 Hz	0.930	0.005
3	MR @ 250 Hz ; R2h @ 32000 Hz ; MR @ 16000 Hz	0.970	0.004

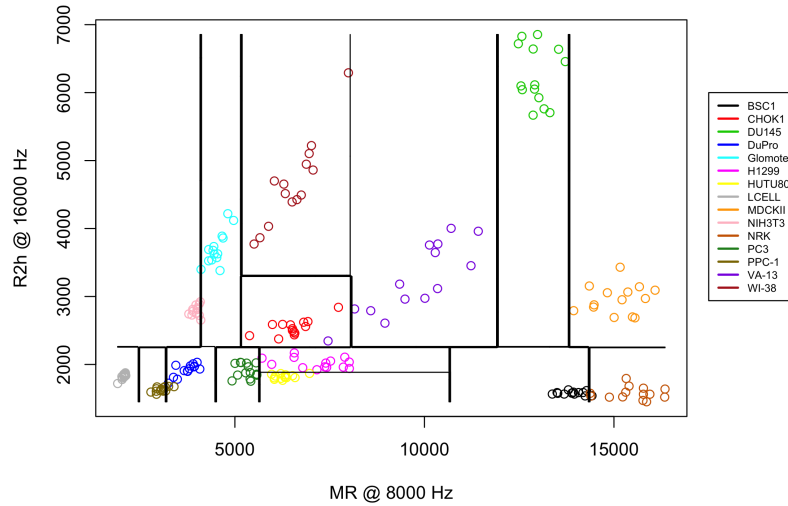
Table 1. Classification Tree Analytical Results: Best feature(s) for cell line classification based on twenty trials of classification tree construction using cells grown on gel serum. Abbreviations are EOR: End of run resistance; MR: Maximum resistance; R2h: Resistance at two hours. The out-of-sample classification rate is the average over all twenty values obtained for each feature. The standard error of this average value is reported in column four. These results show that when classifying cell lines, a 2D feature space is significantly more informative than a 1D feature space. Using three features as opposed to two results in a less drastic improvement in the out-of-sample classification rate, but an improvement nonetheless.

This group of high-performing features is important to consider when interpreting a further implication of Table 1; the table reveals a large increase in the out-of-sample classification accuracy when using an informative pair of features as opposed to an informative single feature. There is a less marked improvement when using a strong trio of features versus a strong pair of features. Lastly, the table suggests that two or three informative features are sufficient to capture the group dynamics of fifteen different cell lines.

Figure 3 offers a visual of the best pair of features proposed in Table 1, and their ability to separate the data with respect to classification trees. In panel (a), we see that the majority of points of the same color reside in the same rectangular region, indicating correct classification. This behavior makes sense given the high out-of-sample classification rate (93%) observed in Table 1.



(a)



(b)

Figure 3. Classification Tree Visual Results: Best pair of features for cell line classification as determined through classification trees using cells grown on gel serum. (a) Example of training/testing set used to conduct classification analysis. Training points are represented by hollow circles, test points represented by x's. Most observations of the same color reside in the same rectangular region, indicating good separation. This behavior corresponds to the high classification accuracy (93%) presented in Table 1. (b) Boundaries created when using all 14 observations in training set (full information).

4.2 Linear and Quadratic Discriminant Analysis

While classification trees, and their horizontal and vertical divisions of the feature space, yielded high out-of-sample classification accuracy, we wanted to see if a more flexible separation of the feature space could produce even better results. Linear and quadratic discriminant analyses seemed appropriate extensions, as they separate the feature space with linear (not necessarily horizontal or vertical) and quadratic divisions, respectively. As both LDA and QDA are special cases of RDA, we reserve the details of their results to Section 4.3 where we discuss RDA at length; this section is meant to provide the mathematical formulation of LDA and QDA for those unfamiliar with the methods.

Formally, LDA assumes that observations X of the κ th class are drawn from the multivariate Gaussian distribution with mean vector μ_k and covariance matrix Σ : ($X \sim \text{Normal}(\mu_k, \Sigma)$). Note the lack of subscript on the covariance matrix; LDA assumes that all K classes have the same covariance structure Σ , a characteristic which distinguishes this method from other classifiers (see QDA below). The LDA algorithm itself is based on Bayesian analysis. Assuming a Gaussian density for the k th class, the Bayes classifier assigns an observation $X = x$ to the class κ for which the posterior probability of x belonging to the κ th class is maximized. This corresponds to assigning an observation $X = x$ to the class κ for which

$$\kappa = \arg \max_k \delta_k(x) = \arg \max_k [x^T \Sigma^{-1} \mu_k - \frac{1}{2} \mu_k^T \Sigma^{-1} \mu_k].$$

The LDA algorithm estimates μ_k and Σ from the training set, which yields estimates for $\hat{\delta}_k(x)$. An observation $X = x^*$ from the testing set is then assigned to the κ th class if $\kappa = \arg \max_k \hat{\delta}_k(x^*)$. The predicted classes using this scheme can then be compared to the true classes to assess classification accuracy [15].

QDA is similar to LDA; QDA assumes that observations X of the κ th class are drawn from the multivariate Gaussian distribution with mean vector μ_k and covariance matrix Σ_k : ($X \sim \text{Normal}(\mu_k, \Sigma_k)$). Here too the Bayes classifier assigns an observation $X = x$ to the

class κ for which the posterior probability of x belonging to the κ th class is maximized. This corresponds to assigning an observation $X = x$ to the class κ for which

$$\kappa = \arg \max_k \delta_k(x) = \arg \max_k \left[-\frac{1}{2}(x - \mu_k)^T \Sigma_k^{-1}(x - \mu_k) \right].$$

Notice here that each of the $k = 1, \dots, K$ classes has its own distinct covariance function, and that the observation x appears in a quadratic form in the Bayes classifier. These are the defining characteristics of QDA. The QDA algorithm estimates μ_k and Σ_k from the training set, which yields estimates for $\hat{\delta}_k(x)$. An observation $X = x^*$ from the testing set is then assigned to the κ th class if $\kappa = \arg \max_k \hat{\delta}_k(x^*)$. As above, the predicted classes using the QDA scheme can then be compared to the true classes to assess classification accuracy [15].

4.3 Regularized Discriminant Analysis

To see if a more flexible separation of the feature space would yield higher classification rates, we performed classification analysis through the RDA algorithm proposed by Friedman [16] on all combinations of features for the gel-based cells. This form of discriminant analysis was appealing for two reasons: first, it allows for a “path” between LDA and QDA which is computationally feasible in high dimensions, and secondly, it has LDA and QDA as special cases. The RDA algorithm begins with computing a convex combination of the group-specific and pooled sample covariance matrices over the k groups in the sample via

$$\hat{\Sigma}_k^{\rho_1} = (1 - \rho_1)\hat{\Sigma}_k + \rho_1\hat{\Sigma}_{\text{pool}},$$

where $0 \leq \rho_1 \leq 1$ is a regularization parameter and $\dim(\hat{\Sigma}_k) = \dim(\hat{\Sigma}_{\text{pool}}) = \{\# \text{ of features in the feature space}\}$. The second step shrinks this estimator towards a multiple of the

identity matrix in the following manner:

$$\hat{\Sigma}_{k,\text{RDA}} = (1 - \rho_2)\hat{\Sigma}_k^{\rho_1} + \frac{\rho_2}{p}\text{tr}(\hat{\Sigma}_k^{\rho_1})\mathbf{I}_p, \quad (3)$$

where $0 \leq \rho_2 \leq 1$ is a second regularization parameter. In equation (3), we note that LDA is achieved when $\rho_1 = 1, \rho_2 = 0$, which corresponds to creating a series of linear divisions of the feature space. We also note that QDA is achieved when $\rho_1 = \rho_2 = 0$, which corresponds to creating a series of quadratic divisions of the feature space. For all other $0 < \rho_1 < 1$ and $\rho_2 = 0$, we have a division of the feature space which is somewhere in between linear and quadratic, hence providing us with a “path” between LDA and QDA. We explored a variety of values of ρ_1 in our analysis, including the special cases of $\rho_1 \in \{0, 1\}$, fixing $\rho_2 = 0$.

To gain an understanding of the effect of different values of ρ_1 on the classification accuracy, we selected values from 0.05 to 0.95 to use in the RDA algorithm on all pairs and trios of features, leaving $\rho_2 = 0$ fixed. To run this algorithm in R, we modified the function `RDA.R` by Aerts and Wilms to accommodate specific values of ρ_1 and ρ_2 [17]. The same random sampling scheme used during the classification tree analysis was adopted here, with half of the data constituting the training set, and the other half forming the test set. Here too we repeated our analysis on twenty different random samplings of the data to mitigate any sensitivity to initialization. Reported accuracy rates for each feature are the average over all twenty of these trials.

As seen in Figure 4, the best performing parameter value for ρ_1 for pairs of features is 0.3. The majority of the ρ_1 values, up until about 0.7, seem to have about the same effect on the classification rate. This is most likely due to the fact that seven out of the top ten features for those ρ_1 values were the same. For trios of features, the selected value for ρ_1 is 0.05 (or 0.15). The effect of different ρ_1 values seems even smaller in this scenario, with the classification rate only changing from 0.983 - 0.992 over the entire range of tested parameter values. It is interesting to note that the best performing ρ_1 values are different for pairs

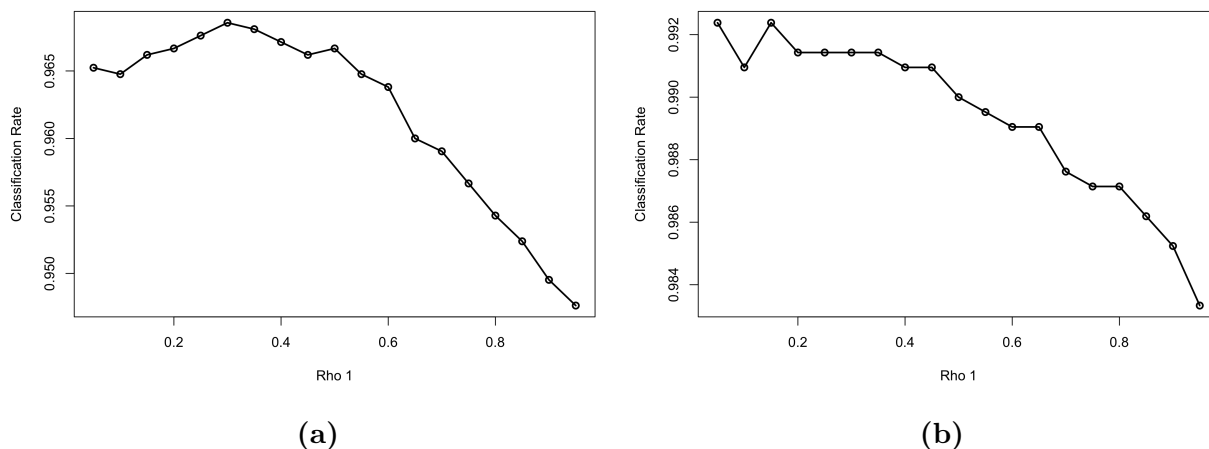


Figure 4. Exploration of ρ_1 for Gel-Based Cells: Classification rate associated with different values of ρ_1 ($\rho_2 = 0$ fixed) using cells grown on gel serum. (a) For pairs of features, the highest rate corresponds to $\rho_1 = 0.3$. (b) For trios of features, the highest rate corresponds with $\rho_1 = 0.05 = 0.15$; however, the range of classification rates is narrow for all tested values of ρ_1 , from 0.983 - 0.992, suggesting the parameter value has a small effect on the outcome in this scenario.

and trios of features, but the overall shape of the curve is the same; classification rates are highest for low ρ_1 values and decrease in an almost linear fashion for larger ρ_1 values.

Figure 5 also offers a visual as to how the different values of ρ_1 divide the feature space, and thus affect the classification rate. For this plot, we ran our RDA analysis with three different values of ρ_1 and a high performing pair of features. The shapes of the regions bounded by the lines associated with each ρ_1 can be quite different. Since the data associated with these two features is so well separated, though, the effect on the classification rate is minimal, with only two or three points falling into incorrect groups as a result of the boundary line changes. This behavior corresponds with that in Figure 4.

We next repeated our RDA analysis with the ideal value of ρ_1 indicated in Figure 4 on all pairs and trios of features, taking $\rho_2 = 0$. Single features were omitted due to a restriction in the `RDA.R` code. Table 2 contains the numerical results of our analysis, while Figure 6 offers a visualization of the feature space characteristic of RDA, somewhere between a linear and quadratic division. Note that these divisions are quite different from those in Figure 3.

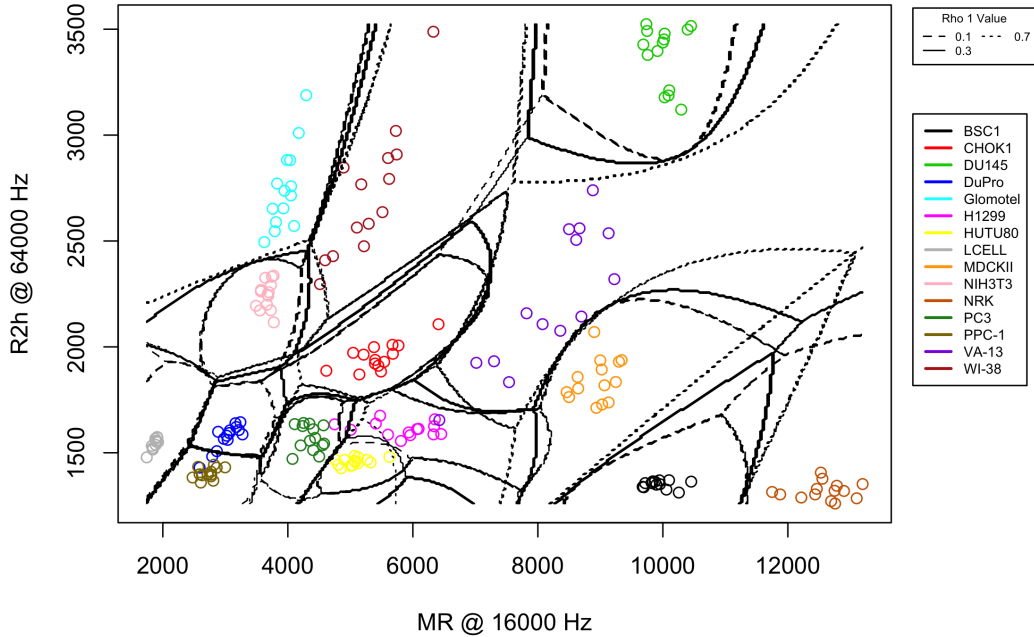


Figure 5. RDA Boundary Changes with ρ_1 : Comparison of feature space division given three different values of ρ_1 in RDA algorithm on an example pair of features ($\rho_2 = 0$ fixed) with cells grown on gel serum. We see only slight changes in the boundaries, suggesting the value of ρ_1 has little impact on the classification rate of the RDA algorithm in this scheme. This observation is also echoed in Figure 4.

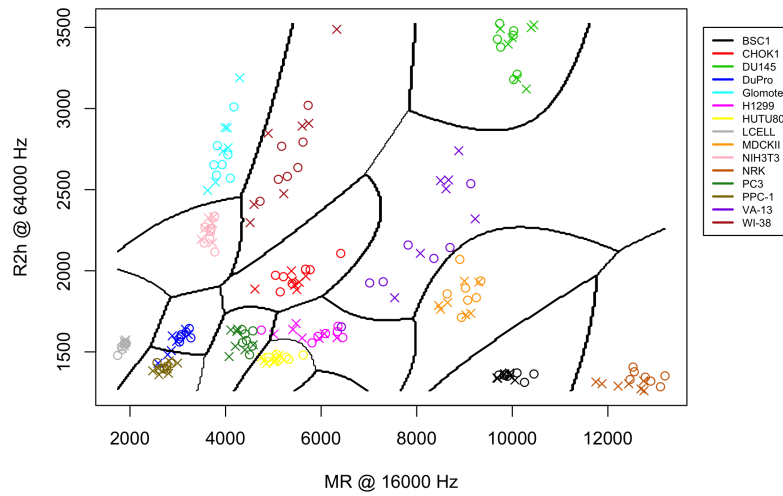
In Table 2 we see these differences correspond to about a 4 percentage point increase in the out-of-sample classification rate for the best pair of features using RDA versus classification trees. We also see an increase of about 2 percentage points for the best trio of features using RDA versus classification trees. We emphasize again, though, that the features highlighted in Table 2 are merely members of a larger set of high-performing features. For example, the pairs R2h @ 32000 Hz ; MR @ 16000 Hz and R2h @ 32000 Hz ; MR @ 8000 Hz have classification accuracies only one 1 percentage point worse than the best pair. What is more, the latter pair is the same pair that yielded the highest classification rate under the classification tree scheme; unfortunately, similar crossover was not found between the highest performing trio of features. So, while not all pairs and trios of features could yield

Feature Space Dimension	Selected Classification Feature(s)	Out-of-Sample Classification Rate	Approximate Standard Error
2	R2h @ 64000 Hz ; MR @ 16000 Hz	0.969	0.004
3	R2h @ 64000 Hz ; MR @ 2000 Hz ; MR @ 64000 Hz	0.992	0.002

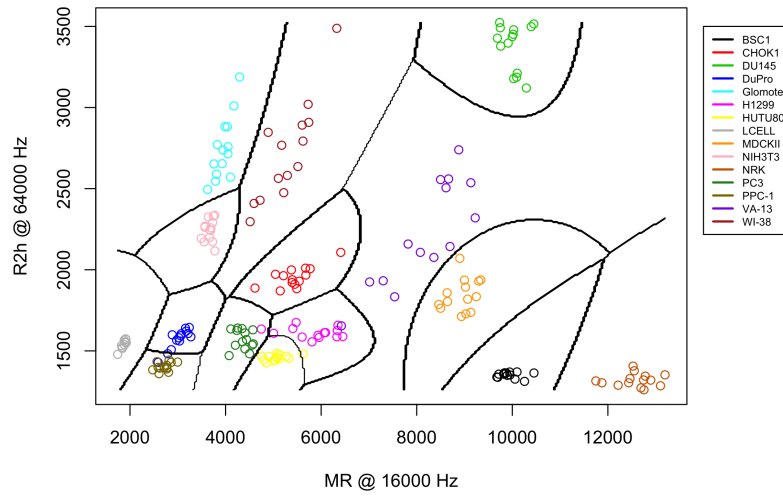
Table 2. RDA Analytical Results: Best features for cell line classification based on twenty trials of RDA with $\rho_1 = 0.3$ for pairs and $\rho_1 = 0.05$ for trios. In both cases, $\rho_2 = 0$ was fixed, and the cells were grown on gel serum. The out-of-sample classification rate is the average over all twenty values obtained for each feature. The standard error of this average value is reported in column four. We see an improvement of several percentage points in the classification rates for both pairs and trios of features, as compared to those from the classification trees.

classification rates as high as 97% and 99%, respectively, there are a number which could perform within just a few percentage points of these values.

Based on our preliminary analysis on the effect of the ρ_1 value on the classification rate, and the low parameter value sensitivity observed, we suspected that the rates associated with LDA and QDA would be similar to those when we specified $\rho_1 \in \{0.05, 0.3\}$, the optimal parameter values for RDA on trios and pairs of features, respectively. As LDA and QDA are common classification techniques, with nice visualization properties, we extended our RDA analysis to account for these two special cases. The same random sampling and averaging techniques were used here as before. Instead of using the `RDA.R` code, we used the `lda()`, `predict.lda()`, `qda()` and `predict.qda()` functions to allow for evaluation of single features, as well as pairs and trios. We verified that the results using the modified `RDA.R` code had the same LDA and QDA results for pairs and trios of features as the `lda()` and `qda()` functions. The numerical and visual results can be found in Tables 3-4 and Figures 7-8, with highlights summarized below.



(a)



(b)

Figure 6. RDA Visual Results: Example of best pair of features for cell line classification as determined through RDA with $\rho_1 = 0.3, \rho_2 = 0$ when cells grown on gel serum. a) Example of training/testing set used to conduct classification analysis. Training points are represented by hollow circles, test points represented by x's. This separation corresponds to about 97% predictive accuracy, as seen in Table 2. (b) Boundaries created when using all 14 observations in training set (full information).

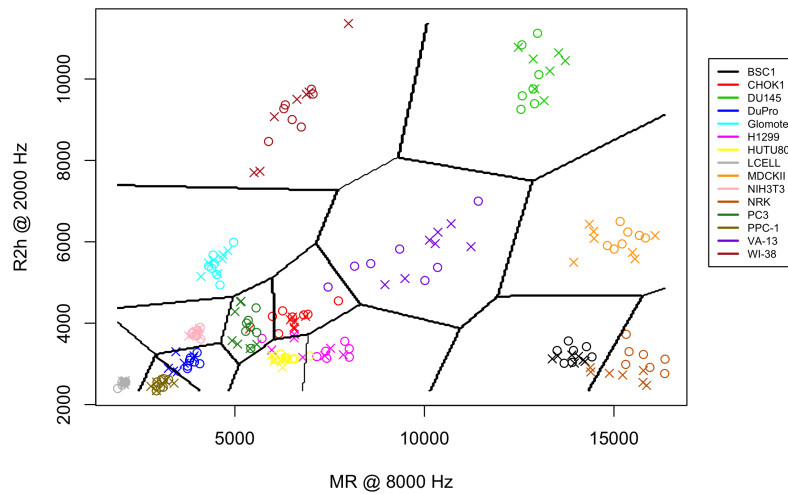
In Tables 3-4 we see a similar selection of EOR, MR, and R2h features in the mid- to high-frequency range. Compared to classification trees, we also see that LDA and QDA offer uniformly higher out-of-sample classification rates for each combination of features. The margin of improvement in this rate is slightly smaller between pairs and trios of features than it was for classification trees. The results for LDA and QDA were nearly identical, particularly for the single and trio set of features. Compared to RDA, all applicable classification rates for LDA and QDA were worse. High-performing features showed some consistency: the best single feature and feature pair under LDA also appeared in the top 10 selected by RDA. The best single feature and feature trio under QDA also appeared in the top 10 selected by RDA.

Feature Space Dimension	Selected Classification Feature(s)	Out-of-Sample Classification Rate	Approximate Standard Error
1	EOR @ 1000 Hz	0.763	0.007
2	R2h @ 2000 Hz ; MR @ 8000 Hz	0.944	0.004
3	MR @ 64000 Hz ; R2h @ 1000 Hz ; MR @ 1000 Hz	0.981	0.003

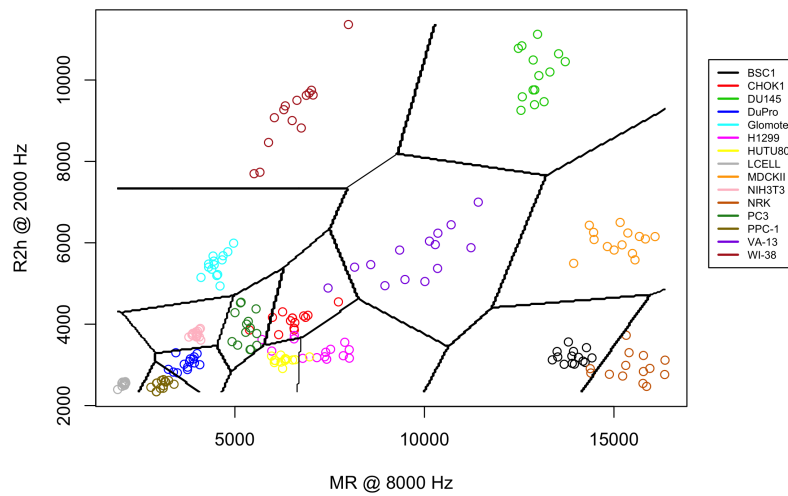
Table 3. LDA Analytical Results: Best feature(s) for cell line classification based on twenty trials of LDA with cells grown on gel serum. The out-of-sample classification rate is the average over all twenty values obtained for each feature. The standard error of this average value is reported in column four. Similar features were selected here as in the classification tree analysis (Table 1). The predictive accuracy rates increased for each combination of features, as compared to Table 1. The margin of improvement in this rate decreased slightly between pairs and trios of features. All rates were worse compared to RDA on gel-based cells, when applicable (Table 2).

Feature Space Dimension	Selected Classification Feature(s)	Out-of-Sample Classification Rate	Approximate Standard Error
1	EOR @ 1000 Hz	0.762	0.005
2	EOR @ 32000 Hz ; EOR @ 16000 Hz	0.951	0.005
3	EOR @ 32000 Hz ; R2h @ 8000 Hz ; R2h @ 4000 Hz	0.978	0.004

Table 4. QDA Analytical Results: Best feature(s) for cell line classification based on twenty trials of QDA with cells grown on gel serum. The out-of-sample classification rate is the average over all twenty values obtained for each feature. The standard error of this average value is reported in column four. These results are almost identical to those from LDA, particularly for the best single feature and trio of features.

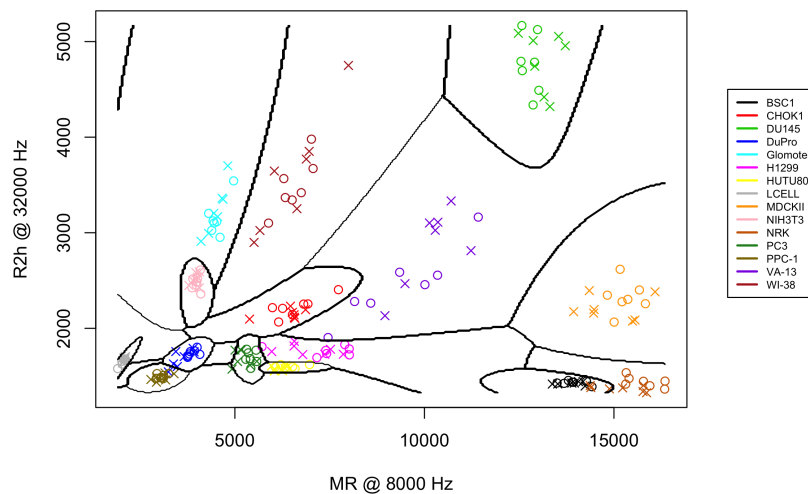


(a)

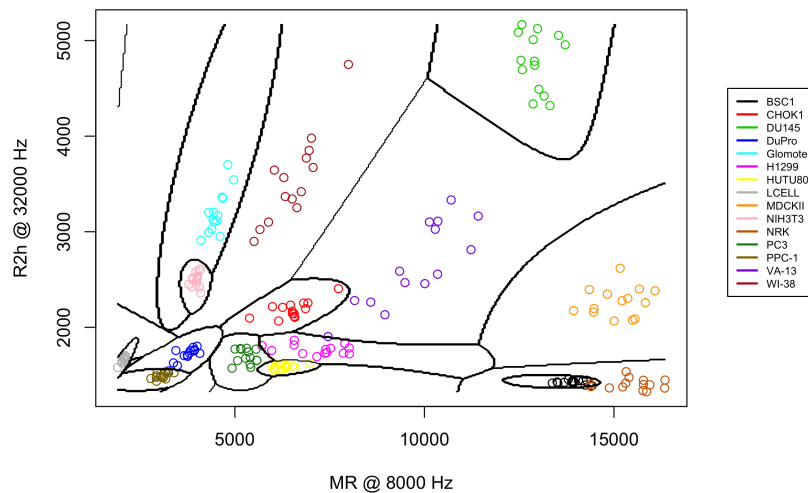


(b)

Figure 7. LDA Visual Results: Best pair of features for cell line classification as determined through LDA with cells grown on gel serum. (a) Example of training/testing set used to conduct classification analysis. Training points are represented by hollow circles, test points represented by x's. Most observations of the same color reside in the same oblong region, indicating good separation. This behavior corresponds to the high classification accuracy ($\approx 94\%$) presented in Table 3. (b) Boundaries created when using all 14 observations in training set (full information).



(a)



(b)

Figure 8. QDA Visual Results: Results obtained using best pair of features for cell line classification as determined through QDA with cells grown on gel serum. (a) Example of training/testing set used to conduct classification analysis. Training points are represented by hollow circles, test points represented by x's. This separation corresponds to about 95% predictive accuracy, as seen in Table 4. (b) Boundaries created when using all 14 observations in training set (full information).

The Figures 7-8 show how LDA and QDA separate the feature space into linear and quadratic regions, respectively. A visual comparison of the LDA, QDA, and RDA regions (in Figures 6-8) shows some similarities; but, the classification rates in the corresponding tables in the manuscript and supplemental materials indicate that RDA is still the superior classification method. Hence, having a more flexible classification algorithm, which allows for a division of the feature space somewhere between linear and quadratic, seems to yield the best results for this data.

4.4 Serum Effect on Classification Rates: BSA vs. Gel

The same analysis that was applied to the cells inoculated in gel serum, as described in Sections 4.1 and 4.3, was repeated on those cells inoculated in BSA serum. Table 5 provides the numeric results of the analysis, while Figures 9-10 provide visualizations. A notable similarity exists between these results and the ones from the gel-based cells. In particular,

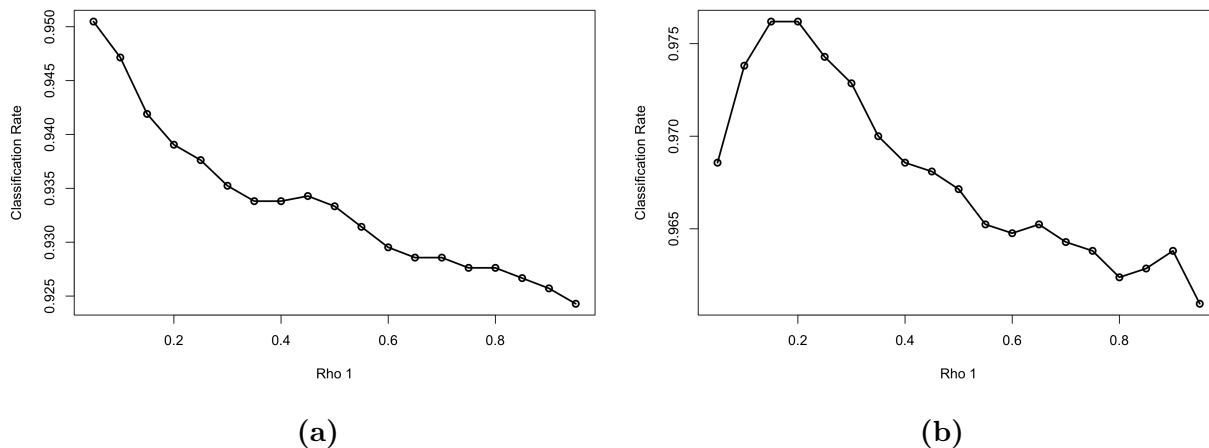


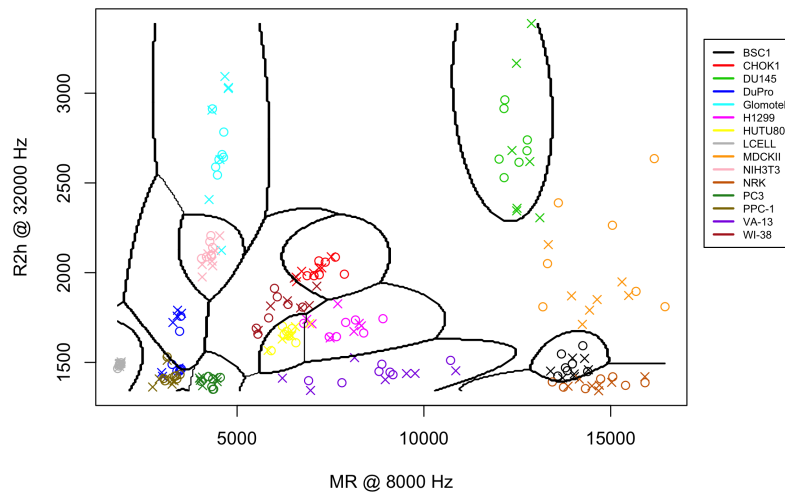
Figure 9. Exploration of ρ_1 for BSA-Based Cells: Classification rate associated with different values of ρ_1 ($\rho_2 = 0$ fixed) using cells grown on BSA serum. (a) For pairs of features, the highest rate corresponds to $\rho_1 = 0.05$. The classification rate range is nearly double that in Figure 4(a), suggesting the ρ_1 values matter more for the BSA-treated cells, as opposed to the gel treated cells, at least for pairs of features. (b) For trios of features, the highest rate corresponds to $\rho_1 = 0.15 = 0.2$. The classification range is also somewhat larger here than in Figure 4(b).

Method	Feature Space Dimension	Selected Classification Feature(s)	Out-of-Sample Classification Rate	Approximate Standard Error
Tree	1	MR @ 1000 Hz	0.680	0.008
	2	R2h @ 4000 Hz ; MR @ 4000 Hz	0.935	0.005
	3	EOR @ 8000 Hz ; R2h @ 16000 Hz ; R2h @ 1000 Hz	0.950	0.004
RDA	1	N/A	N/A	N/A
	($\rho_1 = 0.05$)	EOR @ 16000 Hz ; EOR @ 8000 Hz	0.950	0.005
	($\rho_1 = 0.15$)	R2h @ 250 Hz ; R2h @ 4000 Hz ; MR @ 16000 Hz	0.976	0.003
LDA ($\rho_1 = 1$)	1	EOR @ 2000 Hz	0.724	0.008
	2	R2h @ 2000 Hz ; MR @ 1000 Hz	0.920	0.004
	3	R2H @ 250 Hz ; R2h @ 2000 Hz ; MR @ 2000 Hz	0.960	0.004
QDA ($\rho_1 = 0$)	1	EOR @ 2000 Hz	0.722	0.006
	2	EOR @ 16000 Hz ; EOR @ 8000 Hz	0.950	0.005
	3	R2H @ 4000 Hz ; MR @ 250 Hz ; Alpha	0.963	0.005

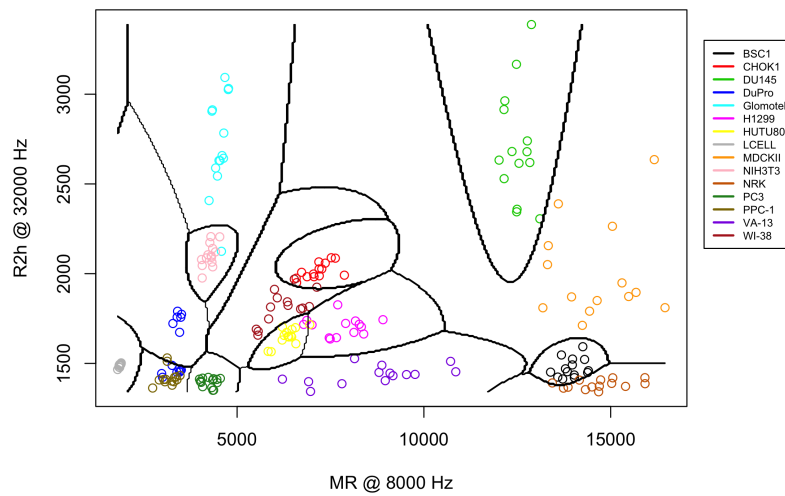
Table 5. All Analytical Results (BSA-Based Cells): Best feature(s) for cell line classification based on twenty trials of various classification methods with cells grown on BSA serum. The out-of-sample classification rate is the average over all twenty values obtained for each feature. The standard error of this average value is reported in column five. The ρ_1 values used in the RDA analysis were the optimal values for each dimension. Compared to the results from cells grown on gel serum, we see nearly uniformly lower out-of-sample classification rates, lower frequencies selected for best features, and the appearance of Alpha as a best feature.

we see that the ordering of best to worst classification methods was the same for both sets of data (RDA with optimal ρ_1 , QDA, LDA, classification trees). If we compare the change in percentage points of the classification accuracy when going from single features, to pairs, to trios of features for each method, though, we do not see this consistency. For example, sometimes the gap between pairs and trios is higher for the BSA-based cells, and sometimes it is lower, depending on the method; no apparent trend is observed.

In all but one case (pairs of features assessed using classification trees), the BSA-based cells had lower classification rates than the gel-based cells for all classification methods. Figure 10 indicates why BSA-based cells were harder to classify; the plot shows that the observations overlapped more between groups, and, within a particular group, the observations were generally more spread out. This behavior may also explain why the value of ρ_1 in the RDA algorithm had a greater effect on the out-of-sample classification rate (see Figure 9); changing the boundaries in Figure 10, as dictated by ρ_1 , would yield more differences than



(a)



(b)

Figure 10. RDA Visual Results for BSA-Based Cells: Results obtained using best pair of features for cell line classification as determined through RDA with $\rho_1 = 0.05$ and $\rho_2 = 0$ with cells grown on BSA serum. a) Example of training/testing set used to conduct classification analysis. This separation corresponds to about 95% predictive accuracy, as seen in Table 5. We see more overlap between cell lines here than we did for those cells inoculated in gel serum. (b) Boundaries created when using all 14 observations in training set (full information).

in Figure 5. Table 5 also suggests that lower frequencies of data, such as 1000 Hz and 2000 Hz, are more informative for BSA-based cells, as opposed to the higher frequencies, such as 16000 Hz and 32000 Hz, which were selected as the best features for the gel-based cells. At this time we are unsure as to whether or not these results suggest a slight advantage to using cells grown on gel serum, as opposed to BSA serum. In future work, we can continue to use both types of cells, comparing separate analyses or combining the two samples to run a larger study.

5 Conclusions

These results have established that previous studies were missing valuable information by only relying on ECIS data obtained from one frequency, typically 4000 Hz. While the tables in this manuscript and the supplemental materials provide only examples of the best feature(s), it was clear that 4000 Hz was not the sole frequency selected. Instead, there seemed to be a fairly consistent set of high-performing features, such as low-frequency EOR for single features, and mid- to high-frequency R2h/MR for pairs of features for gel-based cells, which yielded impressive classification rates across all methods. We also found that previous works were limiting the utility of the features for cell line differentiation by analyzing them on an individual basis. While only incremental improvement in accuracy was gained from considering trios of features, as opposed to pairs of features, there was a marked improvement when considering pairs versus individual features in this experiment. As for the best classification method, our results suggest that RDA with a value of ρ_1 away from the boundary yields the most accurate results. We also note that LDA and QDA offer only small improvements over basic classification trees, a margin which decreases as the number of predictor variables increases.

Overall, results are encouraging for future work. Since we now know the value of utilizing the multi-frequency data offered by ECIS for cell line classification, we will look to extend the

experimental design to allow for a broader feature space. In particular, we will continue to look at cells grown on different serums, and also examine cells wounded by a high frequency current after reaching confluence [9]. We will also obtain more data at a finer temporal resolution during the steady-state stage of growth to study those confluence features proposed in previous studies that we were unable to address in this work. As in this study, we will evaluate each feature, both new and old, at multiple frequencies. We hope that adding these features will enrich the classification algorithm and provide even better cell line separation. Lastly, we note the potential for a two- or three-dimensional final feature space which provides good classification accuracy given our results, making a visualization tool of this classification scheme feasible.

6 Acknowledgements

The authors would like to thank Applied BioPhysics for providing the data and the technical/biological background for this work. Financial support from the Cornell University Institute of Biotechnology, the New York State Division of Science, Technology and Innovation (NYSTAR), a Xerox PARC Faculty Research Award, NSF Award DMS-1455172, and Cornell University Atkinson's Center for a Sustainable Future AVF-2017 is gratefully acknowledged as well.

References

- [1] Ivar Giaever and Charles R Keese. Micromotion of mammalian cells measured electrically. *Proceedings of the National Academy of Sciences*, 88(17):7896–7900, 1991.
- [2] Soumen Das, Analava Mitra, and Rangadhar Pradhan. Characterization of electrode/electrolyte interface of ecis devices. *Electroanalysis*, 24(12):2405–2414, 2012.
- [3] Michael Isaacson, David A Lawrence, Nirankar N Mishra, Donald E Mousseau, Scott Retterer, Donald Szarowski, James N Turner, and Thomas J Zieziulewicz. On-chip micro-biosensor for the detection of human cd4+ cells based on ac impedance and optical analysis. *Biosensors and Bioelectronics*, 21(5):696–704, 2005.
- [4] Soumen Das, Mahitosh Mandal, Analava Mitra, Rangadhar Pradhan, and Shashi Rajput. Electric cell–substrate impedance sensing technique to monitor cellular behaviours of cancer cells. *RSC Advances*, 4(19):9432–9438, 2014.
- [5] Ivar Giaever, Charles R Keese, and Paramitra Mitra. Electric measurements can be used to monitor the attachment and spreading of cells in tissue culture. *BioTechniques*, 11(4):504–510, 1991.
- [6] Ivar Giaever, Charles R Keese, and Chun-Min Lo. Monitoring motion of confluent cells in tissue culture. *Experimental Cell Research*, 204(1):102–109, 1993.
- [7] Eric Huang, Jennifer Lim, Chun-Min Lo, Jun-Chih Lo, Daniel Opp, and Brian Wafu. Use of electric cell–substrate impedance sensing to assess in vitro cytotoxicity. *Biosensors and Bioelectronics*, 24(8):2625–2629, 2009.
- [8] Jennifer Friedman, Chun-Min Lo, Douglas C Lovelady, Sonali Patel, and David A Rabson. Detecting effects of low levels of cytochalasin b in 3t3 fibroblast cultures by analysis of electrical noise obtained from cellular micromotion. *Biosensors and Bioelectronics*, 24(7):2250–2254, 2009.

- [9] Sonja Lukic and Joachim Wegener. Impedimetric monitoring of cell-based assays. *eLS*, 2015.
- [10] Chun-Min Lo, Douglas C Lovelady, Anastasia N Maggi, David A Rabson, and TC Richmond. Distinguishing cancerous from noncancerous cells through analysis of electrical noise. *Physical Review E*, 76(4):041908, 2007.
- [11] Iain M Cockburn, Leonard P Freedman, and Timothy S Simcoe. The economics of reproducibility in preclinical research. *PLoS biology*, 13(6):e1002165, 2015.
- [12] Andreas Janshoff, Angelika Sapper, and Joachim Wegener. Cell motility probed by noise analysis of thickness shear mode resonators. *Analytical Chemistry*, 78(14):5184–5191, 2006.
- [13] Simone M Brandenburg, Irene H Heijink, Jacobien A Noordhoek, Dirkje S Postma, Dirk-Jan Slebos, and Antoon JM van Oosterhout. Characterisation of cell adhesion in airway epithelial cell types using electric cell–substrate impedance sensing. *European Respiratory Journal*, 35(4):894–903, 2010.
- [14] Chang K Choi, Anthony E English, Giljun Park, and Tim E Sparer. Electrical impedance measurements predict cellular transformation. *Cell Biology International*, 33(3):429–433, 2009.
- [15] Trevor Hastie, Gareth James, Rob Tibshirani, and Daniela Witten. *An Introduction to Statistical Learning*. Springer, 2013.
- [16] Jerome H Friedman. Regularized discriminant analysis. *Journal of the American Statistical Association*, 84:165–175, 1989.
- [17] Stéphanie Aerts and Ines Wilms. Code: Cellwise robust regularized discriminant analysis. <https://feb.kuleuven.be/ines.wilms/code%20>, 2017. [Online; accessed 2017-11-01].